How to cite: *Angew. Chem. Int. Ed.* **2021**, *60*, 13529–13535
International Edition: doi.org/10.1002/anie.202101792
German Edition: doi.org/10.1002/ange.202101792

Nanorings | Hot Paper

# Cycloparaphenylene–Phenalenyl Radical and Its Dimeric Double Nanohoop**

*Yong Yang, Olivier Blacque, Sota Sato, and Michal Juríček**

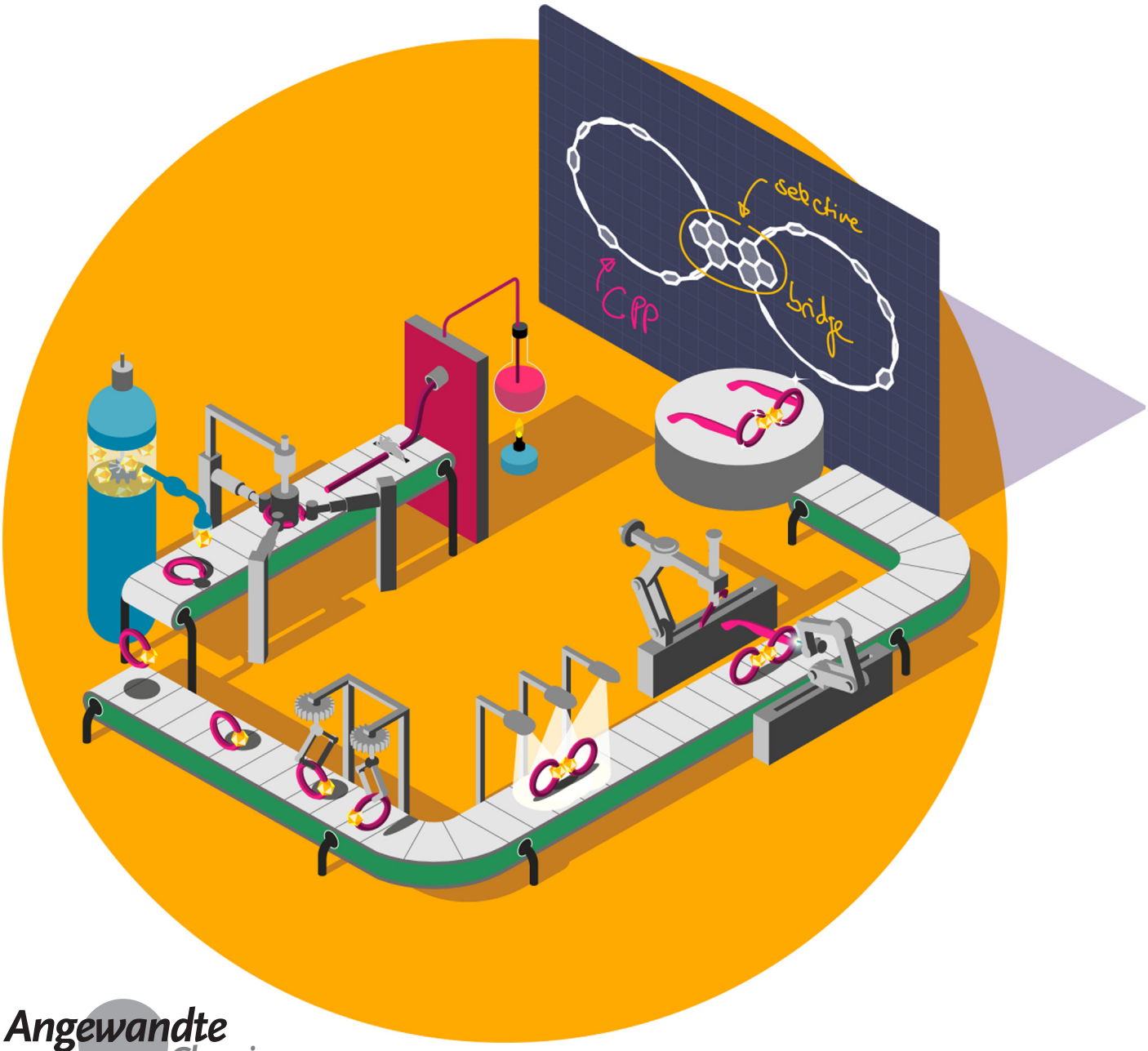


  

***Abstract:*** *The first example of a neutral spin-delocalized carbon-nanoring radical was achieved by integration of the open-shell phenalenyl unit into cycloparaphenylene (CPP). Spin distribution in this hydrocarbon is localized primarily on the phenalenyl segment and partially on the CPP segment as a consequence of steric and electronic effects. The resulting geometry is reminiscent of a diamond ring, with pseudo-perpendicular arrangement of the radial and the planar π-surface. The phenylene rings attached directly to the phenalenyl unit give rise to a steric effect that governs a highly selective dimerization pathway, yielding a giant double nanohoop. Its π-framework made of 158 $sp^2$-carbon atoms was elucidated by single-crystal X-ray diffraction, which revealed a three-segment CPP-peropyrene-CPP structure. This nanocarbon shows a fluorescence profile characteristic of peropyrene, regardless of which segment gets excited. These results in conjunction with DFT suggest that adjusting the size of the CPP segments in this double nanohoop could deliver donor–acceptor systems.*

Open-shell nanographenes[1] characterized by delocalized spin density are synthetic targets of fundamental interest to chemists. They are investigated for their amphoteric redox properties,[2] magnetism[3] and conductivity,[4] and potential applications in spintronics[5] and quantum computing.[6] The prototype of such class of compounds is phenalenyl (**Phen**; Figure 1a), a spin-1/2 odd-alternant neutral hydrocarbon and the smallest triangular graphene fragment.[7] Its characterization by electron paramagnetic resonance (EPR) spectroscopy confirmed its delocalized open-shell electronic structure,[8] where the unpaired π-electron is evenly distributed between six α-positions (Figure 1a). In solution, phenalenyl exists in equilibrium with its σ-dimer,[9] which in the presence of oxygen undergoes a reaction cascade to yield peropyrene as the final product.[10] The reactivity of phenalenyl can be controlled by steric effects[11] or electronically by π-extension,[12] which can lead to a selective reactivity[13] or suppress it.[12] The known π-extended spin-1/2 derivatives of phenalenyl are restricted to planar[1] and helical examples.[13a,14] To explore new structural platforms, we turned our attention to a cylindrical cycloparaphenylene (CPP) framework,[15] which offers an opportunity to control spin distribution and reactivity by a combination of steric and electronic effects.

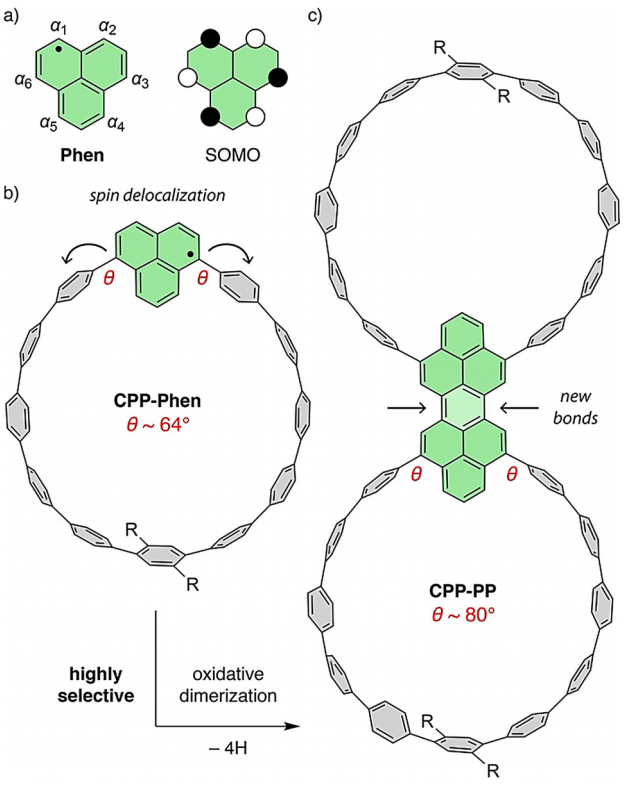


***Figure 1.*** a) Structure of phenalenyl (**Phen**) and hybrid nanocarbons b) **CPP–Phen** and c) **CPP–PP** developed in this work (R = OPr). θ = average dihedral angle between a nanographene segment and the neighboring phenylene ring.

CPPs are structural models[16] and synthetic templates[17] for armchair carbon nanotubes. On account of their curved cyclic π-conjugation and hollow interior, they are attractive synthetic targets in material science and supramolecular chemistry.[18] Their curved geometry weakens the overlap of p orbitals, which gives rise to a partial quinoidal character that increases with decreasing diameter.[19] Quinoidal structures favor delocalization of unpaired electrons, as it does not involve the loss of aromatic stabilization energy, which has been observed in radical cations[20] and anions[21] of CPPs but not in neutral species. Changing the linkage mode of one phenylene ring from *para* to *meta* results in a geometry where the *meta*-phenylene ring lies within the CPP plane perpendicularly to the neighboring *para*-phenylene rings, which disrupts their π-communication.[22] To utilize the potential of CPPs as a platform to control spin distribution and reactivity, we began to explore hybrid nanocarbon systems, comprising open-shell nanographenes integrated within the CPP nanorings.

Herein, we present the prototype of such systems, a CPP-based neutral radical **CPP–Phen** (Figure 1b), in which one phenylene ring of the CPP loop is replaced by a phenalenyl unit connected in a pseudo-*meta*-fashion via two α-positions ($\alpha_3$ and $\alpha_6$). This linkage mode results in a geometry

[*] Dr. Y. Yang, Dr. O. Blacque, Prof. Dr. M. Juríček
Department of Chemistry
University of Zurich
Winterthurerstrasse 190, 8057 Zurich (Switzerland)
E-mail: michal.juricek@chem.uzh.ch
Dr. S. Sato
Department of Applied Chemistry
The University of Tokyo
Hongo, Bunkyo-ku, Tokyo 113-8656 (Japan)

[**] A previous version of this manuscript has been deposited on a preprint server (https://doi.org/10.26434/chemrxiv.13705516.v1).
Supporting information and the ORCID identification numbers for the authors of this article can be found under: https://doi.org/10.1002/anie.202101792.

reminiscent of a diamond ring, where the phenalenyl unit lies in the CPP plane almost perpendicularly to the connecting phenylene rings. Consequently, 1) the majority of spin density resides on the phenalenyl unit and only a part of it extends onto the CPP segment, and 2) the dimerization pathway through the positions $\alpha_3$–$\alpha_6$ of the phenalenyl unit is suppressed. This steric effect leads to a highly selective dimerization via $\alpha_1$- and $\alpha_2$-positions, yielding a double-nanohoop peropyrene (**CPP–PP**; Figure 1c) as the exclusive dimeric product. Notably, **CPP–PP** represents a fully π-conjugated hydrocarbon framework made of 158 $sp^2$-carbon atoms as a novel member of CPP architectures that feature multiple nanoring cycles.[23–27]

The pivotal intermediate in our synthetic strategy was nanoring **1** (Scheme 1), formed by one dihydrophenalenone unit and 11 phenylene rings. It was synthesized via Suzuki–Miyaura cross-coupling macrocyclization of dihydrophenalenone **2** and C-shaped linker **3**. Precursor **2** was prepared starting from trisubstituted naphthalene **4**, which first underwent a selective Kumada cross-coupling to afford **5** in 76% yield. The subsequent Heck coupling and the reduction of the C–C double bond followed by hydrolysis afforded **6** in 71% yield. In the final step, ICl-promoted iodination, acyl chloride formation, and Friedel–Crafts acylation provided **2** in 65% yield. The structure of **2** was determined by single-crystal X-ray diffraction (SC-XRD; Figure S2). The directing angle of the corner linker plays a crucial role in the construction of the cyclic scaffold of CPPs.[15] After screening various candidates, C-shaped linker **3** was found ideal to unite with **2** and afford nanoring **1** in 15% yield upon reductive aromatization. The structure of **1** was unequivocally validated by SC-XRD. The solid-state structure (Figure S3) revealed that the dihydrophenalenone unit is non-coplanar with the neighboring phenylene rings, with the dihedral angles (64° and 67°) significantly larger than those between any two phenylene rings of the CPP segment (avg. 28°). Finally, **1** was subjected to the reduction and dehydration to afford CPP–1*H*-phenalene, the hydroprecursor of **CPP–Phen**.

Upon the addition of *p*-chloranil in toluene at room temperature under a nitrogen atmosphere, the pale-yellow solution of the hydroprecursor rapidly changes color to yellow, then green, and after some time, a dark brown-orange mixture is observed. This observation suggests the "decomposition" pathway of phenalenyl to peropyrene, which involves σ-dimer formation as shown in Scheme 1. Kubo and co-workers identified[10b] all intermediates of this reaction sequence (Scheme S3), which involves three oxidation steps starting from hydroprecursor (−6H). Thus, at least three equivalents of *p*-chloranil had to be used for the full conversion of CPP–1*H*-phenalene to **CPP–PP**. The use of less than three equivalents of *p*-chloranil results in a mixture of all intermediates—these conditions were used for the EPR spectroscopic characterization of **CPP–Phen**. The dimeric product **CPP–PP** was separated and its formation was confirmed with MALDI-TOF MS (Figure S1). **CPP–PP** exhibited a poor solubility in common organic solvents due to its large and rigid structure. It is noteworthy that the total isolated yield of **CPP–PP** starting from **1** is 32%, surpassing that of peropyrene from a pre-dimerized dihydrophenalenone

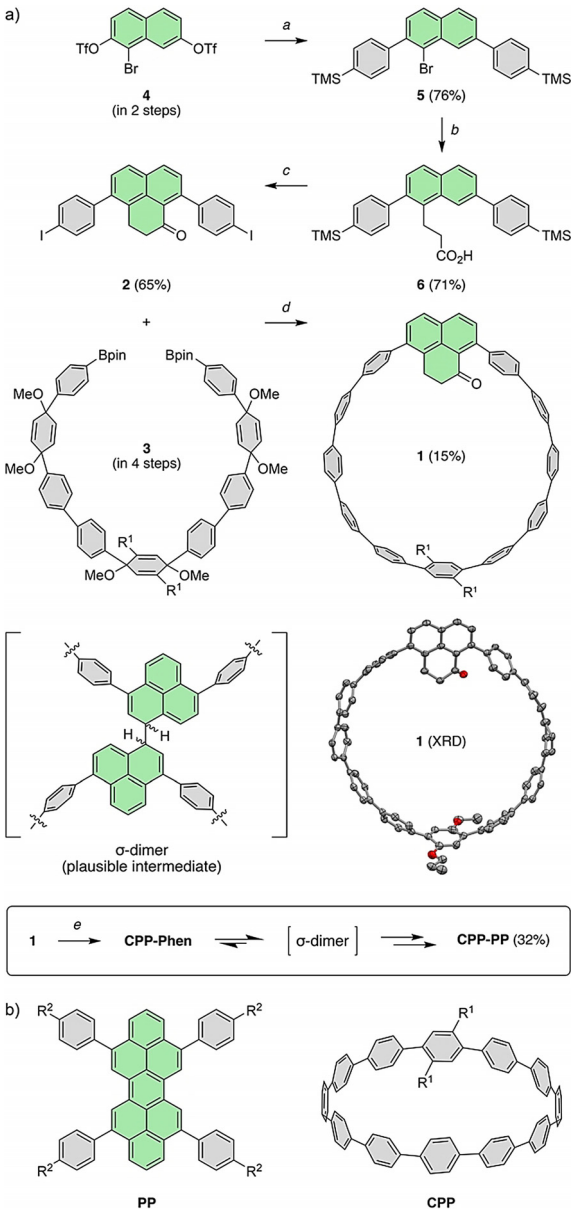


***Scheme 1.*** a) Synthesis of **CPP–Phen** and **CPP–PP**, and the solid-state structure of **1**. Reaction conditions: a) 4-(trimethylsilyl)phenylmagnesium bromide, $PdCl_2$(dppp), LiBr, $Et_2O$, 0°C; b) (i) methyl acrylate, $Pd(OAc)_2$, $PPh_3$, $K_2CO_3$, *n*-$Bu_4NBr$, DMF, 90°C, (ii) $NaBH_4$, $NiCl_2{\cdot}6H_2O$, THF/MeOH, rt, (iii) NaOH, THF/EtOH/$H_2O$, rt; c) (i) ICl, $CCl_4$, 0°C, (ii) oxalyl chloride, $CHCl_3$, reflux, (iii) $AlCl_3$, $CH_2Cl_2$, 0°C; d) (i) SPhos Pd G3, aq. $K_3PO_4$, 1,4-dioxane, 80°C, (ii) $H_2SnCl_4$, THF, rt; e) (i) $NaBH_4$, $CH_2Cl_2$/EtOH, rt, (ii) *p*-toluenesulfonic acid monohydrate, toluene, 90°C, (iii) *p*-chloranil, toluene, rt. b) Structures of **PP** and **CPP**. $R^1$ = OPr, $R^2$ = 3,5-di-*tert*-butylphenyl.

(< 22%).[10b] This facile π-skeletal expansion from **CPP–Phen** to **CPP–PP** represents a novel synthetic tactic to achieve double nanohoop architectures, distinct from the conventional synthesis of lemniscate CPPs, where the bridging building block is constructed prior to the macrocyclization.[23] In addition, to better understand the photophysical properties of **CPP–PP**, two segments of it, namely, **CPP** and **PP** (Scheme 1b), were synthesized and fully characterized including SC-XRD (see the Supporting Information).

  

The paramagnetic nature of **CPP–Phen** was probed by EPR spectroscopy. A diluted toluene solution of CPP–1*H*-phenalene and *p*-chloranil (1:1, ca. $10^{-3}$ M) gave a well-resolved 16-peak-multiplet EPR spectrum at 307 K (Figure 2d) with a *g* value of 2.0039, which is typical for delocalized spin-1/2 hydrocarbon radicals. This spectrum was simulated[28] as a quartet of a pentet (qp) using proton hyperfine coupling constants (*hcc*) of 6.10 G (four α-protons) and 1.95 G (three β-protons).[29] This splitting pattern is in accord with DFT calculations, which reveal that the majority of spin density is localized on the phenalenyl unit (Figure 2b,c). The simulated *hcc* values agree well with the calculated ones (Figure 2a, ca. 6.5 G for α- and ca. 2.4 G for β-protons). Based on DFT, the two neighboring phenylene rings possess dramatically smaller *hcc* values (0.27–0.58 G), which are not resolved in the experimental spectrum. This spin distribution can be rationalized by a pseudo-perpendicular arrangement between the phenalenyl unit and the phenylene rings, which is favored for units with a *meta*-linkage.[22] The steric preference for a perpendicular arrangement acts against the electronic preference for a coplanar arrangement, which is ideal for spin-delocalization onto the phenylene rings. This "clash of forces" is supported by the calculated dihedral angles (avg. ca. 64°, Figure S10), which are smaller compared to **CPP–PP** (avg. ca. 80°, Figure 3a), and by comparing **CPP–Phen** to its strain-free linear analog (Figures S5 and S12), which displays a higher degree of spin density on the phenylene rings.

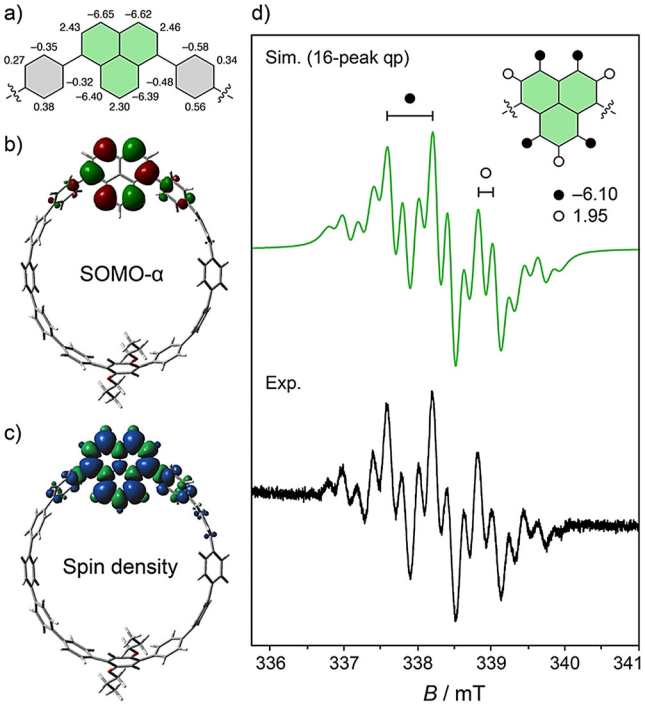


***Figure 2.*** a) Calculated (DFT, UB3LYP/EPR-III on UB3LYP/6-31G(d,p) geometry) proton hyperfine coupling constants (*hcc*/G), b) singly occupied molecular orbital (SOMO-α), and c) spin-density distribution of **CPP-Phen**. d) Simulated (line width = 1.4 G) and experimental (toluene, 307 K) EPR spectra of **CPP–Phen** (qp = quartet of pentet).

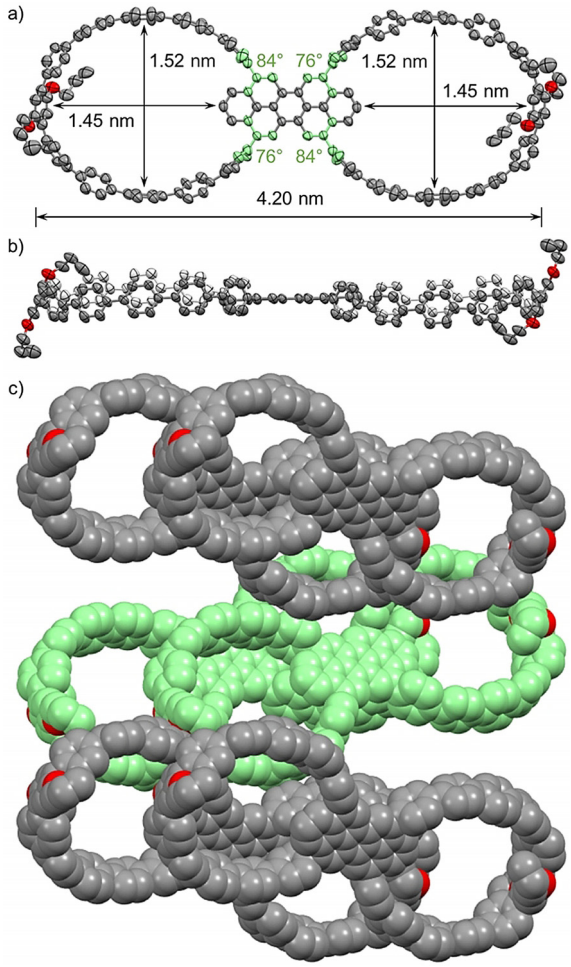


***Figure 3.*** Solid-state structure of **CPP–PP**:[34] a) top and b) side view (the thermal ellipsoids are shown at the 25% probability level), c) packing structure along the *c* axis. Disordered solvent molecules are omitted for clarity.

The XRD analysis of **CPP–PP** unambiguously confirmed its fully π-conjugated framework with a $C_2$ symmetry, where the peropyrene segment serves as a rigid bridge between two CPP segments. The dihedral angles at the four linkages are approximately 80° on average (Figure 3a, green), implying a radial-planar-radial alignment of the π-conjugated segments. The length reaches 4.20 nm and the two cavities have an oval shape with a short axis of 1.52 nm. The distance between the protons of the peropyrene segment and the opposite phenylene rings is 1.45 nm, which implies that the cavities of **CPP–PP** might be suited for the encapsulation of fullerenes.[30] No evidence of binding $C_{60}$ or $C_{70}$, however, was observed, which suggests that the cavities are not an ideal fit. The herringbone packing structure is similar to that of most CPP molecules[30a] (Figure 3c).

The photophysical properties of **CPP**, **PP**, and **CPP–PP** were investigated in $CHCl_3$ solutions (Figure 4). **CPP** showed only one intense absorption band at 342 nm, which is nearly identical to that of parent [12]CPP.[31] According to time-dependent (TD)-DFT calculations, the HOMO→LUMO ($S_0 \rightarrow S_1$) transition is weakly allowed with $f = 0.283$, and the major contributions for the observed band are HOMO−1→

  

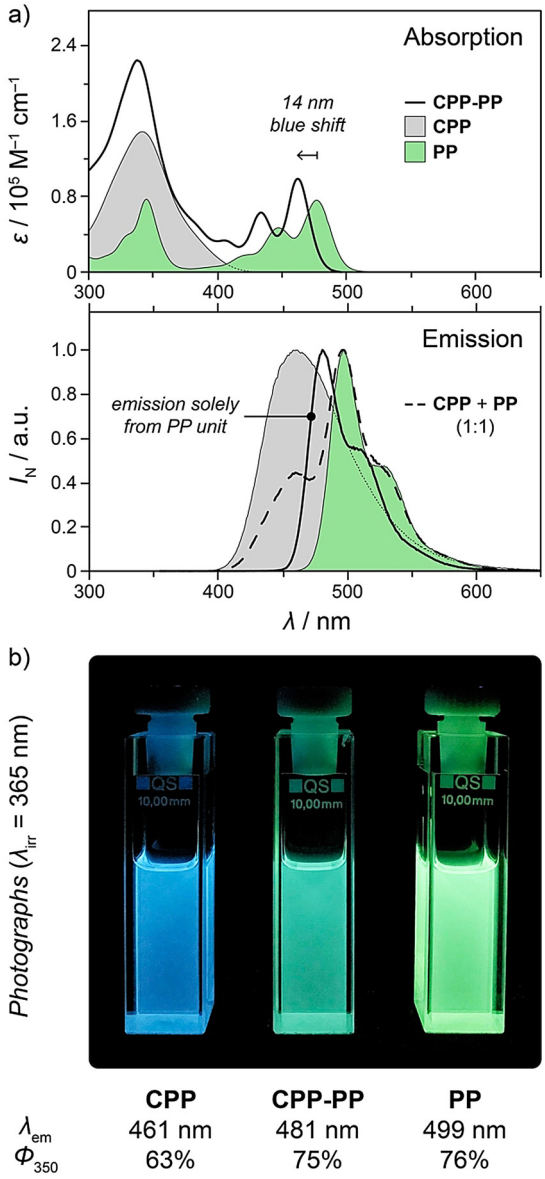


***Figure 4.*** a) UV/Vis absorption and fluorescence spectra of **CPP–PP** ($\lambda_{ex}$ = 338 nm), **CPP** ($\lambda_{ex}$ = 342 nm), **PP** ($\lambda_{ex}$ = 345 nm), and a 1:1 mixture of **CPP** and **PP** ($\lambda_{ex}$ = 344 nm) in $CHCl_3$ at 25 °C. b) Photographs of the $CHCl_3$ solutions of **CPP–PP**, **CPP**, and **PP** under irradiation at 365 nm.

LUMO ($S_0 \rightarrow S_2$, $f = 2.30$) as well as HOMO−2→LUMO and HOMO→LUMO + 1 ($S_0 \rightarrow S_3$, $f = 3.26$) transitions (Figure S17). **PP** exhibited the most intense band at 345 nm, and two less intense bands at 447 and 477 nm, which are characteristic of the peropyrene backbone (HOMO→LUMO ($S_0 \rightarrow S_1$, $f = 1.47$) transition, Figure S18).[32] **CPP–PP** showed an absorption spectrum that represents a superposition of those of **CPP** and **PP**, except a minor shift (Figure 4a). The dominant absorption band at 338 nm is primarily derived from the absorption of two CPP segments, and it can be ascribed to multiple HOMO−$n$→LUMO + $m$ transitions ($n$ = 0–7, $m$ = 0–11; $S_0 \rightarrow S_5$, $f = 4.46$; $S_0 \rightarrow S_7$, $f = 4.43$; Figure S19), including CPP-localized (e.g., HOMO−3→LUMO + 2) and charge-transfer transitions (e.g., HOMO→LUMO + 5). In addition, the two typical absorption bands of the peropyrene segment were observed at 434 nm and 463 nm (HOMO→LUMO ($S_0 \rightarrow S_1$, $f = 2.15$) transition), blue-shifted by 14 nm compared to those of **PP**. This blue shift is due to the weaker conjugation between the peropyrene and CPP segments, as indicated by the significantly larger dihedral angles at the four linkages (avg. 80°, Figure 3a) compared to those of **PP** (avg. 57°, Figure S4).

The profile of the fluorescence spectrum of **CPP–PP** is almost identical to that of **PP**, except a blue shift of 18 nm, without any contribution from **CPP** (Figure 4). For a comparison, a 1:1 mixture of **CPP** and **PP** shows a fluorescence profile which represents the superposition of the individual spectra of both components. The fluorescence quantum yields for **CPP**, **PP**, and **CPP–PP** in $CHCl_3$ are 0.63, 0.76, and 0.75, respectively (excitation of 350 nm, Figure S7). These results indicate an efficient internal conversion from the $S_n$ ($n > 1$) states to the $S_1$ state in **CPP–PP**.

To conclude, we synthesized the first example of a neutral spin-delocalized carbon-nanoring radical and demonstrated that the radially π-conjugated CPP framework is a unique structural platform to control spin distribution and reactivity of spin-delocalized systems such as phenalenyl via the interplay of steric and electronic effects. Our results lay the groundwork for future research towards the understanding of spin-delocalization through a radially π-conjugated backbone. For example, CPP–phenalenyl systems with a pseudo-*para* connection mode (via an α- and a β-position of phenalenyl) and a smaller ring size of the CPP segment are expected to favor a quinoidal over a benzenoid structure[19] and thus lead to a more extended spin-delocalization. These concepts can be applied to understand through-space or guest-mediated spin interactions in multi-spin-unit and host–guest CPP systems, respectively. The selective dimerization of the nanoring radical to the double nanohoop represents a novel synthetic approach towards CPP architectures with non-coplanar arrangements of π-surfaces such as the radial-planar-radial array mode. Our photophysical and DFT studies suggest that decreasing the size of the CPP segments in our double nanohoop, and thus lowering the HOMO–LUMO gap, could deliver donor–acceptor systems.[33] We believe that investigation of other members of this novel family of non-planar open-shell hydrocarbon radicals will have implications in the fields of material science, spintronics, and supramolecular chemistry.

## Acknowledgements

This project received funding from the European Research Council (ERC) under the European Union's Horizon 2020 research and innovation programme (Grant Agreement No. 716139) and the Swiss National Science Foundation (SNSF, PP00P2_170534). We are grateful to Prof. Greta Patzke, Lukas Reith, and Leoš Valenta (University of Zurich) for help with EPR measurements, to Dr. Tomáš Šolomek (University of Bern) for helpful discussions, and to KEK Photon Factory for the access to the X-ray diffraction instrument, BL-17A beamline (2019G051).

  

## Conflict of interest

The authors declare no conflict of interest.

**Keywords:** cycloparaphenylene · fluorescence · nanohoop · phenalenyl · spin-delocalization


[1] a) T. Kubo, *Chem. Rec.* **2015**, *15*, 218 – 232; b) Y. Morita, S. Suzuki, K. Sato, T. Takui, *Nat. Chem.* **2011**, *3*, 197 – 204; c) A. Konishi, T. Kubo in *Chemical Science of π-Electron Systems* (Eds.: T. Akasaka, A. Osuka, S. Fukuzumi, H. Kandori, Y. Aso), Springer, Tokyo, **2015**, pp. 337 – 360; d) W. Zeng, J. Wu, *Chem* **2021**, *7*, 358 – 386.

[2] a) T. Kubo, K. Yamamoto, K. Nakasuji, T. Takui, I. Murata, *Bull. Chem. Soc. Jpn.* **2001**, *74*, 1999 – 2009; b) Y. Morita, S. Nishida, T. Murata, M. Moriguchi, A. Ueda, M. Satoh, K. Arifuku, K. Sato, T. Takui, *Nat. Mater.* **2011**, *10*, 947 – 951.

[3] a) N. Pavliček, A. Mistry, Y. Majzik, N. Moll, G. Meyer, D. J. Fox, L. Gross, *Nat. Nanotechnol.* **2017**, *12*, 308 – 312; b) S. Mishra, D. Beyer, K. Eimre, J. Liu, R. Berger, O. Gröning, C. A. Pignedoli, K. Müllen, R. Fasel, X. Feng, P. Ruffieux, *J. Am. Chem. Soc.* **2019**, *141*, 10621 – 10625; c) J. Su, M. Telychko, P. Hu, G. Macam, P. Mutombo, H. Zhang, Y. Bao, F. Cheng, Z.-Q. Huang, Z. Qiu, S. J. R. Tan, H. Lin, P. Jelínek, F.-C. Chuang, J. Wu, J. Lu, *Sci. Adv.* **2019**, *5*, eaav7717.

[4] a) S. K. Pal, M. E. Itkis, F. S. Tham, R. W. Reed, R. T. Oakley, R. C. Haddon, *Science* **2005**, *309*, 281 – 284; b) T. Kubo, A. Shimizu, M. Sakamoto, M. Uruichi, K. Yakushi, M. Nakano, D. Shiomi, K. Sato, T. Takui, Y. Morita, K. Nakasuji, *Angew. Chem. Int. Ed.* **2005**, *44*, 6564 – 6568; *Angew. Chem.* **2005**, *117*, 6722 – 6726; c) R. C. Haddon, *Nature* **1975**, *256*, 394 – 396.

[5] a) M. Slota, A. Keerthi, W. K. Myers, E. Tretyakov, M. Baumgarten, A. Ardavan, H. Sadeghi, C. J. Lambert, A. Narita, K. Müllen, L. Bogani, *Nature* **2018**, *557*, 691 – 695; b) Z. Bullard, E. C. Girão, J. R. Owens, J. W. A. Shelton, V. Meunier, *Sci. Rep.* **2015**, *5*, 7634 – 7634; c) O. V. Yazyev, *Rep. Prog. Phys.* **2010**, *73*, 056501; d) D. Pesin, A. H. MacDonald, *Nat. Mater.* **2012**, *11*, 409 – 416.

[6] a) F. Lombardi, A. Lodi, J. Ma, J. Liu, M. Slota, A. Narita, W. K. Myers, K. Müllen, X. Feng, L. Bogani, *Science* **2019**, *366*, 1107 – 1110; b) B. Trauzettel, D. V. Bulaev, D. Loss, G. Burkard, *Nat. Phys.* **2007**, *3*, 192 – 196.

[7] a) K. Uchida, T. Kubo, *J. Synth. Org. Chem. Jpn.* **2016**, *74*, 1069 – 1077; b) D. H. Reid, *Q. Rev. Chem. Soc.* **1965**, *19*, 274 – 302.

[8] P. B. Sogo, M. Nakazaki, M. Calvin, *J. Chem. Phys.* **1957**, *26*, 1343 – 1345.

[9] a) Z. Mou, K. Uchida, T. Kubo, M. Kertesz, *J. Am. Chem. Soc.* **2014**, *136*, 18009 – 18022; b) K. Uchida, Z. Mou, M. Kertesz, T. Kubo, *J. Am. Chem. Soc.* **2016**, *138*, 4665 – 4672; c) K. Uchida, Y. Hirao, H. Kurata, T. Kubo, S. Hatano, K. Inoue, *Chem. Asian J.* **2014**, *9*, 1823 – 1829.

[10] a) S. Pogodin, I. Agranat, *J. Am. Chem. Soc.* **2003**, *125*, 12829 – 12835; b) K. Uchida, S. Ito, M. Nakano, M. Abe, T. Kubo, *J. Am. Chem. Soc.* **2016**, *138*, 2399 – 2410.

[11] K. Goto, T. Kubo, K. Yamamoto, K. Nakasuji, K. Sato, D. Shiomi, T. Takui, M. Kubota, T. Kobayashi, K. Yakusi, J. Y. Ouyang, *J. Am. Chem. Soc.* **1999**, *121*, 1619 – 1620.

[12] a) T. Kubo, Y. Katada, A. Shimizu, Y. Hirao, K. Sato, T. Takui, M. Uruichi, K. Yakushi, R. C. Haddon, *J. Am. Chem. Soc.* **2011**, *133*, 14240 – 14243; b) Q. Xiang, J. Guo, J. Xu, S. Ding, Z. Li, G. Li, H. Phan, Y. Gu, Y. Dang, Z. Xu, Z. Gong, W. Hu, Z. Zeng, J. Wu, Z. Sun, *J. Am. Chem. Soc.* **2020**, *142*, 11022 – 11031.

[13] a) P. Ravat, P. Ribar, M. Rickhaus, D. Haussinger, M. Neuburger, M. Juríček, *J. Org. Chem.* **2016**, *81*, 12303 – 12317; b) P. Ravat, O. Blacque, M. Juríček, *J. Org. Chem.* **2020**, *85*, 92 – 100.

[14] a) A. Ueda, H. Wasa, S. Suzuki, K. Okada, K. Sato, T. Takui, Y. Morita, *Angew. Chem. Int. Ed.* **2012**, *51*, 6691 – 6695; *Angew. Chem.* **2012**, *124*, 6795 – 6799; b) F. Tani, M. Narita, T. Murafuji, *ChemPlusChem* **2020**, *85*, 2093 – 2104.

[15] Selected reviews of CPPs: a) H. Omachi, Y. Segawa, K. Itami, *Acc. Chem. Res.* **2012**, *45*, 1378 – 1389; b) S. E. Lewis, *Chem. Soc. Rev.* **2015**, *44*, 2221 – 2304; c) E. R. Darzi, R. Jasti, *Chem. Soc. Rev.* **2015**, *44*, 6401 – 6410; d) D. Wu, W. Cheng, X. Ban, J. Xia, *Asian J. Org. Chem.* **2018**, *7*, 2161 – 2181.

[16] a) Y. Segawa, A. Yagi, K. Matsui, K. Itami, *Angew. Chem. Int. Ed.* **2016**, *55*, 5136 – 5158; *Angew. Chem.* **2016**, *128*, 5222 – 5245; b) Y. Segawa, H. Ito, K. Itami, *Nat. Rev. Mater.* **2016**, *1*, 15002.

[17] H. Omachi, T. Nakayama, E. Takahashi, Y. Segawa, K. Itami, *Nat. Chem.* **2013**, *5*, 572 – 576.

[18] a) E. J. Leonhardt, R. Jasti, *Nat. Rev. Chem.* **2019**, *3*, 672 – 686; b) Y. Xu, B. Wang, R. Kaur, M. B. Minameyer, M. Bothe, T. Drewello, D. M. Guldi, M. von Delius, *Angew. Chem. Int. Ed.* **2018**, *57*, 11549 – 11553; *Angew. Chem.* **2018**, *130*, 11723 – 11727; c) Y. Xu, R. Kaur, B. Wang, M. B. Minameyer, S. Gsänger, B. Meyer, T. Drewello, D. M. Guldi, M. von Delius, *J. Am. Chem. Soc.* **2018**, *140*, 13414 – 13420.

[19] K. Tahara, Y. Tobe, *Chem. Rev.* **2006**, *106*, 5274 – 5290.

[20] a) E. Kayahara, T. Kouyama, T. Kato, H. Takaya, N. Yasuda, S. Yamago, *Angew. Chem. Int. Ed.* **2013**, *52*, 13722 – 13726; *Angew. Chem.* **2013**, *125*, 13967 – 13971; b) M. R. Golder, B. M. Wong, R. Jasti, *Chem. Sci.* **2013**, *4*, 4285 – 4291; c) E. Kayahara, T. Kouyama, T. Kato, S. Yamago, *J. Am. Chem. Soc.* **2016**, *138*, 338 – 344.

[21] a) A. V. Zabula, A. S. Filatov, J. Xia, R. Jasti, M. A. Petrukhina, *Angew. Chem. Int. Ed.* **2013**, *52*, 5033 – 5036; *Angew. Chem.* **2013**, *125*, 5137 – 5140; b) S. N. Spisak, Z. Wei, E. Darzi, R. Jasti, M. A. Petrukhina, *Chem. Commun.* **2018**, *54*, 7818 – 7821; c) Z. Zhou, Z. Wei, T. A. Schaub, R. Jasti, M. A. Petrukhina, *Chem. Sci.* **2020**, *11*, 9395 – 9401.

[22] T. C. Lovell, C. E. Colwell, L. N. Zakharov, R. Jasti, *Chem. Sci.* **2019**, *10*, 3786 – 3790.

[23] For CPP-based lemniscates, see: a) Z.-A. Huang, C. Chen, X.-D. Yang, X.-B. Fan, W. Zhou, C.-H. Tung, L.-Z. Wu, H. Cong, *J. Am. Chem. Soc.* **2016**, *138*, 11144 – 11147; b) W. Xu, X.-D. Yang, X.-B. Fan, X. Wang, C.-H. Tung, L.-Z. Wu, H. Cong, *Angew. Chem. Int. Ed.* **2019**, *58*, 3943 – 3947; *Angew. Chem.* **2019**, *131*, 3983 – 3987; c) K. Senthilkumar, M. Kondratowicz, T. Lis, P. J. Chmielewski, J. Cybińska, J. L. Zafra, J. Casado, T. Vives, J. Crassous, L. Favereau, M. Stępień, *J. Am. Chem. Soc.* **2019**, *141*, 7421 – 7427; d) T. A. Schaub, E. A. Prantl, J. Kohn, M. Bursch, C. R. Marshall, E. J. Leonhardt, T. C. Lovell, L. N. Zakharov, C. K. Brozek, S. R. Waldvogel, S. Grimme, R. Jasti, *J. Am. Chem. Soc.* **2020**, *142*, 8763 – 8775.

[24] For double-CPP segments of carbon nanotubes, see: a) J. Xia, M. R. Golder, M. E. Foster, B. M. Wong, R. Jasti, *J. Am. Chem. Soc.* **2012**, *134*, 19709 – 19715; b) Y. Ishii, S. Matsuura, Y. Segawa, K. Itami, *Org. Lett.* **2014**, *16*, 2174 – 2176; c) K. Li, Z. Xu, H. Deng, Z. Zhou, Y. Dang, Z. Sun, *Angew. Chem. Int. Ed.* **2021**, *60*, 7649 – 7653; *Angew. Chem.* **2021**, *133*, 7727 – 7731.

[25] For CPP-based propellers, see: P. Li, L. N. Zakharov, R. Jasti, *Angew. Chem. Int. Ed.* **2017**, *56*, 5237 – 5241; *Angew. Chem.* **2017**, *129*, 5321 – 5325.

[26] For CPP-based carbon nanocages, see: a) K. Matsui, Y. Segawa, K. Itami, *J. Am. Chem. Soc.* **2014**, *136*, 16452 – 16458; b) E. Kayahara, T. Iwamoto, H. Takaya, T. Suzuki, M. Fujitsuka, T. Majima, N. Yasuda, N. Matsuyama, S. Seki, S. Yamago, *Nat. Commun.* **2013**, *4*, 2694; c) S. Cui, G. Zhuang, D. Lu, Q. Huang, H. Jia, Y. Wang, S. Yang, P. Du, *Angew. Chem. Int. Ed.* **2018**, *57*, 9330 – 9335; *Angew. Chem.* **2018**, *130*, 9474 – 9479.

[27] For CPP-based catenanes, see: a) W. Zhang, A. Abdulkarim, F. E. Golling, H. J. Räder, K. Müllen, *Angew. Chem. Int. Ed.* **2017**, *56*, 2645 – 2648; *Angew. Chem.* **2017**, *129*, 2689 – 2692;


  

b) Y.-Y. Fan, D. Chen, Z.-A. Huang, J. Zhu, C.-H. Tung, L.-Z. Wu, H. Cong, *Nat. Commun.* **2018**, *9*, 3037; c) Y. Segawa, M. Kuwayama, Y. Hijikata, M. Fushimi, T. Nishihara, J. Pirillo, J. Shirasaki, N. Kubota, K. Itami, *Science* **2019**, *365*, 272 – 276; d) Y. Segawa, M. Kuwayama, K. Itami, *Org. Lett.* **2020**, *22*, 1067 – 1070.

[28] D. R. Duling, *J. Magn. Reson. Ser. B* **1994**, *104*, 105 – 110.

[29] A total of 20 peaks should be observed. Because the *hcc* value for the β-protons is approximately one third of that for the α-protons, 16 peaks are observed in both the simulated and measured EPR spectra.

[30] a) Y. Xu, M. von Delius, *Angew. Chem. Int. Ed.* **2020**, *59*, 559 – 573; *Angew. Chem.* **2020**, *132*, 567 – 582; b) D. Lu, Q. Huang, S. Wang, J. Wang, P. Huang, P. Du, *Front. Chem.* **2019**, *7*, 668.

[31] R. Jasti, J. Bhattacharjee, J. B. Neaton, C. R. Bertozzi, *J. Am. Chem. Soc.* **2008**, *130*, 17646 – 17647.

[32] V. M. Nichols, M. T. Rodriguez, G. B. Piland, F. Tham, V. N. Nesterov, W. J. Youngblood, C. J. Bardeen, *J. Phys. Chem. C* **2013**, *117*, 16802 – 16810.

[33] a) T. Kuwabara, J. Orii, Y. Segawa, K. Itami, *Angew. Chem. Int. Ed.* **2015**, *54*, 9646 – 9649; *Angew. Chem.* **2015**, *127*, 9782 – 9785; b) E. R. Darzi, E. S. Hirst, C. D. Weber, L. N. Zakharov, M. C. Lonergan, R. Jasti, *ACS Cent. Sci.* **2015**, *1*, 335 – 342; c) J. M. Van Raden, E. R. Darzi, L. N. Zakharov, R. Jasti, *Org. Biomol. Chem.* **2016**, *14*, 5721 – 5727.

[34] CCDC-2060251(**2**), 2060255 (**1**), 2060261 (**CPP**), 2060262 (**PP**) and 2060263 (**CPP-PP**) contain the supplementary crystallographic data for this paper. These data are provided free of charge by the joint Cambridge Crystallographic Data Centre and Fachinformationszentrum Karlsruhe Access Structures service www.ccdc.cam.ac.uk/structures.

Manuscript received: February 4, 2021
Accepted manuscript online: February 26, 2021
Version of record online: April 9, 2021

  